

# A first-order Mott transition in $\text{Li}_x\text{CoO}_2$

C. A. MARIANETTI<sup>1</sup>, G. KOTLIAR<sup>2</sup> AND G. CEDER<sup>1,3\*</sup>

<sup>1</sup>Department of Materials Science and Engineering, Massachusetts Institute of Technology, Cambridge, Massachusetts 02139, USA

<sup>2</sup>Center for Materials Theory, Department of Physics and Astronomy, Rutgers University, Piscataway, New Jersey 08854, USA

<sup>3</sup>Center for Materials Science and Engineering, Massachusetts Institute of Technology, Cambridge, Massachusetts 02139, USA

\*e-mail: gceder@mit.edu

Published online: 22 August 2004; doi:10.1038/nmat1178

Despite many years of experimental searches for a first-order Mott transition in crystalline-doped semiconductors, none have been found. Extensive experimental work has characterized a first-order metal–insulator transition in  $\text{Li}_x\text{CoO}_2$ , the classic material for rechargeable Li batteries, with a metallic state for  $x < 0.75$  and insulating for  $x > 0.95$ . Using density functional theory calculations on large supercells, we identify the mechanism of this heretofore anomalous metal–insulator transition as a Mott transition of impurities. Density functional theory demonstrates that for dilute Li-vacancy concentrations, the vacancy binds a hole and forms impurity states yielding a Mott insulator. The unique feature of  $\text{Li}_x\text{CoO}_2$  as compared with traditional doped semiconductors, such as Si:P, is the high mobility of the Li vacancies, which allows them to rearrange into two distinct phases at the temperature of the metal–insulator transition.

Layered  $\text{CoO}_2$ -based materials are continuing to prove themselves rich in both fundamental physics and technological applications.  $\text{Na}_x\text{CoO}_2$  and its hydrated counterpart are receiving renewed interest due to the discovery of superconductivity<sup>1</sup>, in addition to anomalous thermoelectric properties<sup>2</sup>.  $\text{Li}_x\text{CoO}_2$  is the primary cathode material in rechargeable Li batteries, sustaining a multibillion-dollar market. As a result, it has been the subject of intense experimental and theoretical study, including the prediction<sup>3–5</sup> and experimental verification<sup>6,7</sup> of unusually complex phase behaviour. In this letter, another fundamentally important phenomenon is uncovered within this technologically important material. Using density functional theory (DFT) calculations, we provide firm evidence that  $\text{Li}_x\text{CoO}_2$  exhibits a clear example of a first-order Mott transition in a crystalline-doped semiconductor. Although Mott predicted such transitions to be first-order, all known examples in doped semiconductors are continuous due to the frozen-in random placement of the impurities<sup>8,9</sup>.  $\text{Li}_x\text{CoO}_2$  is distinctly different in that the Li vacancies (that is, the impurities) are highly mobile and may therefore equilibrate.

$\text{Li}_x\text{CoO}_2$  forms a layered structure with Li residing between layers of edge-sharing  $\text{CoO}_6$  octahedra. When  $\text{Li}_x\text{CoO}_2$  is fully lithiated,  $x = 1$ , Co is formally in the 3+ valence state. The crystal field splits the Co-3d states into a lower manifold containing three levels ( $t_{2g}$  states) and a higher manifold containing two levels ( $e_g$  states).  $\text{Co}^{3+}$  exists in the low spin  $t_{2g}^6 e_g^0$  configuration and  $\text{LiCoO}_2$  is a band insulator. Because of the high mobility of Li in this material, it is possible to remove Li either by chemical<sup>10</sup> or electrochemical means<sup>11</sup>. This ability to exchange Li gives  $\text{Li}_x\text{CoO}_2$  its excellent properties as a Li storage material in rechargeable Li batteries<sup>11,12</sup>. Li removal creates a variety of phase transitions in the material including order/disorder transitions<sup>3,11,13</sup>, oxygen sliding<sup>14</sup> and alkali staging<sup>3,6</sup>. Our focus in this paper is on the metal–insulator transition that occurs when small amounts of Li are removed from  $\text{LiCoO}_2$  (ref. 15).

Electronically, Li removal from  $\text{LiCoO}_2$  leads to the creation of holes in the  $t_{2g}$  valence band of  $\text{Li}_x\text{CoO}_2$ . Conductivity measurements indicate that there is a composition-dependent activation barrier for  $x > 0.95$ , which increases as  $x$  approaches one, ranging from a minimum of less than 10 meV to a maximum of 100–300 meV (refs 15,16). X-ray diffraction studies of  $\text{Li}_x\text{CoO}_2$  indicate a two-phase coexistence for  $0.75 < x < 0.95$  (ref. 15). The two coexisting phases are very similar, with the same symmetry, but a 0.7% difference in the c lattice parameter,

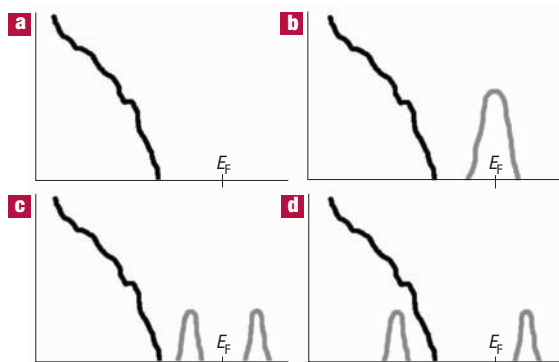


**Figure 1** A schematic of the density-of-states for various realizations of the impurity band. The black curve is the valence band and the grey curve is the impurity band.  $E_F$  denotes the Fermi energy. **a**, Pure band insulator. **b**, Lightly doped band insulator with a metallic impurity band. **c**, Lightly doped band insulator with a Mott insulating impurity band in which the gap is between the lower and upper Hubbard impurity band. **d**, Same as **c** except one of the Hubbard bands has split into the valence band.

which is perpendicular to the layers, and no appreciable difference in the  $a$  lattice parameter (hexagonal setting)<sup>17</sup>. Li-NMR yields a unique NMR signal for each phase, indicating an electronically different Li environment in both phases<sup>15</sup>. The signal for the phase with low Li composition ( $x < 0.75$ ) is Knight-shifted indicating metallic behaviour. Alternatively, the signal for the high Li composition ( $x > 0.95$ ) has no shift, but its intensity decreases as  $x$  decreases from 1 to 0.95. This decrease in intensity is attributed to the presence of a localized spin that interacts strongly with the Li nuclear spin, and shifts a fraction of the NMR signal outside the observable range. Based on these experiments it has been concluded<sup>15</sup> that the system is metallic for  $x < 0.75$ , whereas for  $x > 0.95$  the system contains weakly bound carriers. Hence, the two-phase coexistence for  $0.95 < x < 0.75$  is the result of a first-order metal–insulator transition.

The first step in understanding the transition is to identify the mechanism that induces the insulating state for high Li concentrations ( $x > 0.95$ ).  $\text{LiCoO}_2$  is a band insulator with the Fermi level between the filled  $t_{2g}$  states and the unfilled  $e_g$  states, and one could naively expect a metallic state for  $x < 1$ . Given that the insulating state only has a dilute concentration of holes (<5%), the on-site Co  $t_{2g}$  interactions are not directly relevant as the double occupation of holes on the same site is unlikely. Therefore, polarons or the electrostatic potential of the Li vacancy must be responsible for the localization of the hole. As will be shown below, DFT calculations indicate that the vacancy potential is a dominant factor in localizing the holes. The impurity potential may cause localization in two different ways. First, if the impurity potential is arranged randomly, Anderson localization may occur<sup>18</sup>. However, Anderson transitions are known to be continuous and experiment dictates that the metal–insulator transition under investigation is first-order. The second way in which the impurity potential can cause localization is through the formation of a correlated impurity band. If the vacancy potential is strong enough, it will bind the hole resulting in an impurity band that breaks away from the top of the valence band. This is analogous to what occurs in the classic doped semiconductors, such as Si:P (ref. 19), and Fig. 1 illustrates possible scenarios for this impurity band. For  $\text{LiCoO}_2$ , the valence band is full (Fig. 1a). When the system is lightly doped, an impurity band may form, resulting in a small peak separated from the top of the valence band. This band would be half-filled because there is one hole per vacancy

(Fig. 1b). If an impurity band forms, it is possible that the on-site correlations within the impurity band will be strong enough to split the impurity band and form a Mott insulator (see Fig. 1c and d).

DFT can be used to search for the formation of an impurity band for dilute concentrations of vacancies. All DFT calculations in this paper were performed using the Vienna Ab-initio Simulation Package (VASP)<sup>20,21</sup> within the local-density approximation (LDA). VASP solves the Kohn–Sham equations using projector augmented wave pseudopotentials<sup>22,23</sup> and a plane-wave basis set with a cut-off energy of 400 eV. In the present calculations, we are investigating the nature of the insulating phase,  $x > 0.95$ , and therefore large supercells are required to attain dilute concentration of vacancies. Large-scale parallel computation was performed to reach a minimum concentration of 0.78% vacancies, corresponding to a cell with 511 atoms. A primitive cell with vectors:

$$V_1 = \left( \frac{a\sqrt{3}}{2}, \frac{-a}{2}, 0 \right), \quad V_2 = \left( \frac{a\sqrt{3}}{2}, \frac{a}{2}, 0 \right), \quad V_3 = \left( \frac{-a\sqrt{3}}{6}, \frac{-a}{2}, c \right),$$

where  $a$  is the nearest-neighbour Co distance and  $c$  is the distance between Co planes, was used to generate  $3 \times 3 \times 2$ ,  $4 \times 4 \times 2$ ,  $5 \times 5 \times 2$ ,  $6 \times 6 \times 2$ ,  $7 \times 7 \times 2$ ,  $8 \times 8 \times 2$  supercells containing a single vacancy apiece. Inspecting the top edge of the LDA non-spin-polarized valence density of states (DOS), the formation of a separate peak can clearly be observed as the vacancy concentration is decreased (see Fig. 2). The peak grows more distinct as the vacancy concentration is decreased, culminating in an impurity band that is barely split-off from the valence DOS for 0.78% vacancies. Therefore, LDA calculations indicate the formation of an impurity band, similar to that pictured in Fig. 1a. Non-spin-polarized LDA calculations will always give a half-filled metallic impurity band (Fig. 1b) as opposed to a Mott-insulating impurity band (Fig. 1c or d) given that LDA does not properly treat the electronic correlations. Allowing for spin polarization (the local spin-density approximation, LSDA) in the 1.39% vacancy calculation demonstrates that the ferromagnetic interactions split the impurity band and produce a ferromagnetic insulator (similar to Fig. 1d). This can be considered as analogous to the Hartree–Fock approximation producing a ferromagnetic insulator for the Hubbard model. However, the spin-polarized and non-spin-polarized states are essentially degenerate in energy. The key result is that the LDA produces an impurity band. This band would probably be split in the dilute limit considering that the impurity bandwidth at 0.78% is roughly 20 meV, whereas the experimental conductivity demonstrates that the activation energy of the hole is an order of magnitude larger. Supercells with larger extent along the  $c$  axis were also explored, but it was found that the impurity-band formation was most sensitive to the impurity distance within the  $x$ – $y$  plane. For example, the impurity band is more pronounced for a  $6 \times 6 \times 2$  supercell as compared with a  $5 \times 5 \times 3$  supercell, despite the fact that the former is actually less dilute. This reflects the anisotropic nature of this layered material and more effective screening within the  $x$ – $y$  plane. Given that the system is so dilute in the region of interest (that is,  $x > 0.95$ ), it is certain that there will be some degree of disorder in the system at room temperature. However, the Li vacancies will certainly maximize their spacing because the interactions are repulsive. Therefore, our supercell calculations should be a reasonably accurate representation of impurity-band formation in the experimental system.

To better characterize the nature of the impurity state, we can plot the hole density that has been added to the system as Li is removed. This can be done by subtracting the charge density of the structure with Li vacancies from that of stoichiometric  $\text{LiCoO}_2$ , while holding all structural parameters constant. Figure 3 shows the result for  $\text{Li}_{0.969}\text{CoO}_2$  (3.1% vacancies). The impurity state that is formed by the vacancy potential can be seen as hole density that congregates around the vacancy, and it displays a rather complex structure. The most notable feature is the dominant hole character on the oxygen  $p$  orbitals that

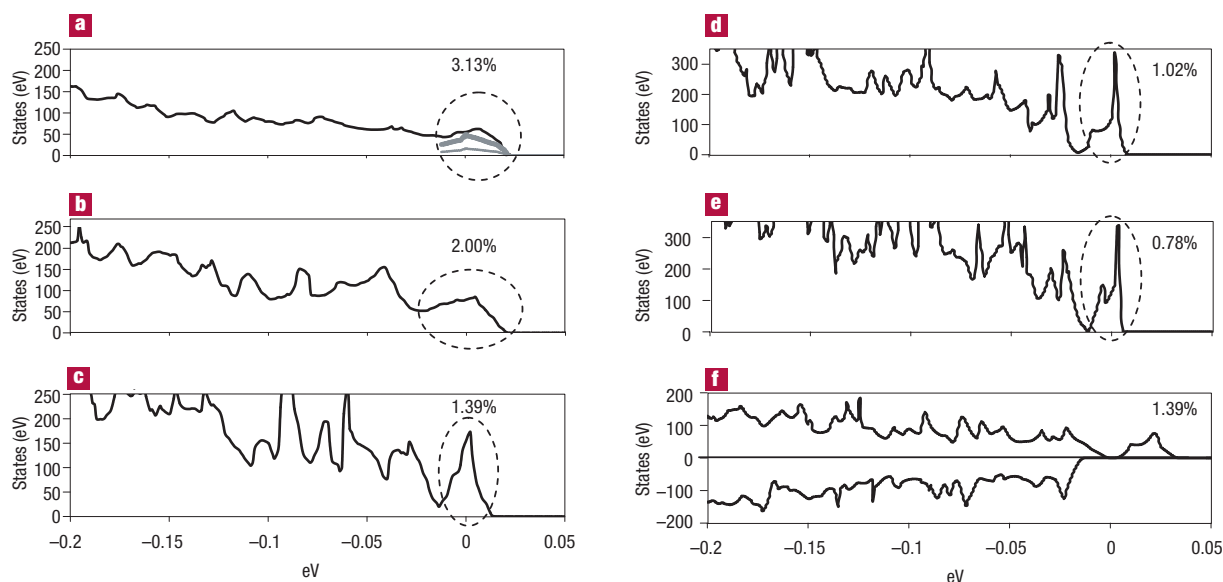


**Figure 2** LDA DOS for various supercells. The Fermi energy is zero in all plots. The impurity band is circled for clarity. All plots are non-spin-polarized with the exception of **f**. **a**,  $4 \times 4 \times 2$  unit cell, 3.13% vacancies. Oxygen and Co partial DOS for the impurity band are shown as thin and thick grey lines, respectively. **b**,  $5 \times 5 \times 2$  unit cell, 2.00% vacancies. **c**,  $6 \times 6 \times 2$  unit cell, 1.39% vacancies. **d**,  $7 \times 7 \times 2$  unit cell, 1.02% vacancies. **e**,  $8 \times 8 \times 2$  unit cell, 0.78% vacancies. **f**,  $6 \times 6 \times 2$  unit cell, 1.39% vacancies.

surround the vacancy. Additionally, electron density can be identified within the  $e_g$  orbitals and hole density within the  $t_{2g}$  orbitals on the Co atoms surrounding the Li vacancy. Given that the projection of the DOS indicates a predominant Co character within the impurity band (see Fig. 2a), it is not immediately obvious why such a strong oxygen character is observed in the charge-density difference plot. This phenomenon has been previously observed in  $\text{LiCoO}_2$  (refs 3, 24, 25) and studied in greater detail in  $\text{Na}_x\text{CoO}_2$  (ref. 26). It is referred to as a rehybridization mechanism, and it results from a competition between the  $e_g$ -oxygen hybridization and the on-site Co Coulomb interaction.

The above LDA calculations suggest that the insulating state is a Mott insulator of impurity states, and therefore it is useful to represent the low-energy physics of the insulating phase as an effective half-filled Hubbard model of impurity states. As the vacancy concentration within the insulating phase is varied, the effective Hubbard model remains half-filled but two distinct effects will modify the electronic structure. First, the centre of gravity of the impurity band will move towards the  $t_{2g}$  bands as the vacancy concentration increases. This is due to the fact that the larger hole density will more effectively screen the vacancy potential. Secondly, the hopping parameters among the vacancy sites (that is, the impurity bandwidth) will increase as the increasing vacancy concentration decreases the average inter-vacancy distance. This will reduce the splitting between the upper and lower Hubbard impurity band. Both effects can independently cause a transition to the metallic state though in a qualitatively different manner. In the first case, the screening of the vacancy potential causes the impurity band to decompose and its states to merge with the  $t_{2g}$  bands once a sufficient hole density is achieved. We refer to this as a classic Mott transition. In the second case, the intra-impurity band-hopping parameters will increase as a function of doping and will eventually overcome the impurity on-site coulomb interaction, giving a metallic impurity band as in Fig. 1a. Given that this is a metal-insulator transition within an always half-filled band we refer to it as a Mott-Hubbard transition. Clearly, a necessary requirement for the Mott-Hubbard transition is that the impurity band persists and is not first destroyed by the classic

Mott mechanism. The composition dependence of the activation energy for electronic conductivity of  $\text{Li}_x\text{CoO}_2$  can be qualitatively understood in terms of the above mechanisms. The excitation gap for carriers will either be between the upper and lower Hubbard impurity band, or between the lower Hubbard impurity band and the valence band if the upper Hubbard band lies within the valence band (see Fig. 1c and d, respectively). In the first scenario, the increase in the intra-impurity hopping parameters will decrease the gap, whereas in the second case both the increase in the intra-impurity hopping and the screening of the impurity potential will reduce the gap.

Having established the nature of the insulating state and the different mechanisms by which it may be destabilized, we now address the first-order transition to the metallic state. If the metal-insulator transition in  $\text{Li}_x\text{CoO}_2$  were a Mott-Hubbard transition, it could be modelled with a one-band Hubbard model. However, this one-band assumption does not appear to be valid in this material. The two-phase region spans 5–25% vacancies, and therefore once more than 5% vacancies are present, a new metallic phase with 25% vacancies will nucleate and grow at the expense of the insulating phase as the vacancy content is further increased. It is therefore unlikely that the impurity band exists in the metallic phase given that it forms at 25% vacancies. This is supported by our calculations, which indicate that the impurity band is barely distinguishable at 3% vacancies. On the contrary, our calculations indicate that the metallic phase can be well described with  $t_{2g}$  states at the Fermi level, in which the impurity band has decomposed and the role of the vacancy has been reduced due to screening. Therefore, the transition in  $\text{Li}_x\text{CoO}_2$  appears to be best characterized as a classic Mott transition, in which the impurity band decomposes due to screening of the vacancy potential by the long-range coulomb interaction of the hole density. Now that the qualitative nature of this transition is understood, we investigate whether or not LDA shows any sign of predicting a first-order transition by looking for a non-convexity in the energy as a function of vacancy content. The LDA should do reasonably well in describing the energetics of the metallic phase, while it probably does not properly describe the energetics of the Mott

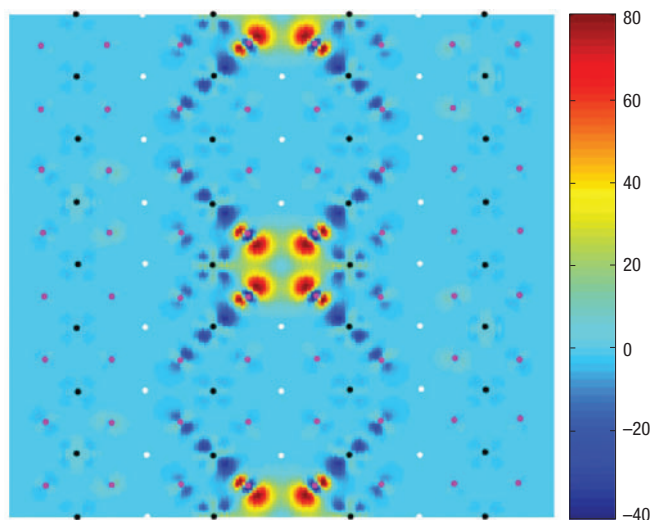


**Figure 3** The total charge-density difference of  $\text{Li}_{0.999}\text{CoO}_2 - \text{CoO}_2$ . A plane that cuts through the Co–O octahedral plane was chosen. Co and O atoms are designated by black and purple dots, respectively, and Li are represented by white dots. The columns of Li/Li-vacancies, O and Co are evident. The Li vacancies are easily identified in the centre of the plot and at the centre of the top and bottom edges. Units are electrons per  $\text{Å}^3$ .

insulating state. We plot the formation energy for the cases of 3.1% and 5.6% vacancies along with the previously published formation energies (see Fig. 4). As shown, the formation energy is nearly linear in the dilute limit and there is no sign of non-convexity. Therefore, although LDA produces an insulating state for low vacancy concentrations, it fails in capturing the first-order nature of the metal–insulator transition. Most likely this failure occurs because LDA does not correctly describe the energetics of the Mott insulating phase correctly. In terms of the effective Hubbard model of the impurity band, one might suggest that LDA is similar to a Hartree–Fock solution of this Hubbard model whereas the true solution would give a correlation-induced splitting that would be lower in energy. Therefore the LDA energies should be pulled down for  $x > 0.95$  and this could create the non-convexity and hence the two-phase region. Another possible source of error in the insulating phase is the possibility that the LDA does not properly describe the formation of the impurity band due to the well known fact that LDA does not properly localize charge. Additionally, a polaron could assist in forming the impurity band by enhancing the effective mass of the holes. However, there is no *a priori* reason to expect the electron–phonon coupling to be large in this situation given that the symmetry of the  $t_{2g}$  states is already broken. All of the above factors will help stabilize the insulating phase and therefore help create the non-convexity. Now that the qualitative nature of this transition is understood and it is clear that LDA fails, it is evident that capturing this transition within a first-principles approach will be challenging. The low-energy electronic degrees of freedom exist on a different length scale for the metal and the insulator. The insulating state is characterized in terms of coarse impurity states that span many oxygen and Co ions, whereas the metallic phase is characterized in terms of finer Co  $t_{2g}$  states. Quantitatively describing this transition will serve as a great challenge to new theoretical techniques, such as cluster dynamical mean-field theory (DMFT)<sup>27,28</sup>, GW+DMFT<sup>29,30</sup>, and typical-medium theory<sup>31</sup>.

One of Mott's early suggestions was to search for the Mott transition in the classic doped semiconductors<sup>32</sup>. Despite the extensive amount of experiments that have been performed on crystalline-doped

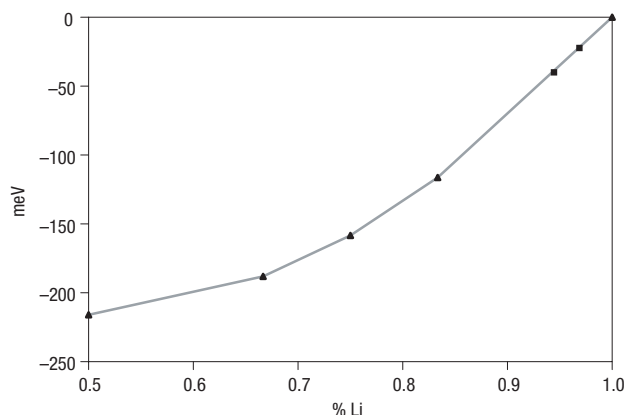


**Figure 4** Total energy of  $\text{Li}_x\text{CoO}_2$ . Previously published calculations by Van der Ven *et al.*<sup>3</sup> are given by triangles, and our calculations by squares.

semiconductors, all of the observed metal–insulator transitions are continuous transitions as opposed to first order<sup>8,9</sup>. This is typically attributed to the random distribution of the impurity states, which creates Anderson localization and destroys the first-order nature of the transition<sup>8</sup>. Perhaps the only exceptions occur in solutions such as  $\text{NaNH}_3$ , where there are experimentally observed first-order transitions that are believed to be associated with a Mott transition<sup>33</sup>. Mott suggested that the high mobility in these solutions may allow the impurities to form a higher degree of order than can be achieved in low-mobility crystalline materials such as Si:P, and perhaps this suppresses the Anderson transition and gives a first-order Mott transition<sup>33</sup>. Therefore, the high mobility of the Li vacancy may be the key difference relative to Si:P, which allows the transition to be first-order. Thus it appears that a very commonly used material such as  $\text{Li}_x\text{CoO}_2$  displays the long-awaited example of a first-order Mott transition in a crystalline-doped semiconductor. Furthermore,  $\text{Li}_x\text{CoO}_2$  should be considered as a new prototype material for studying the interplay between correlation and disorder in which the impurities are highly mobile.

Received 20 February 2004; accepted 8 June 2004; published 22 August 2004.

#### References

1. Takada, K. *et al.* Superconductivity in two-dimensional  $\text{CoO}_2$  layers. *Nature* **422**, 53–55 (2003).
2. Terasaki, I., Sasago, Y. & Uchinokura, K. Large thermoelectric power in  $\text{NaCo}_2\text{O}_4$  single crystals. *Phys. Rev. B* **56**, 12685–12687 (1997).
3. Van der Ven, A., Aydinol, M. K., Ceder, G., Kresse, G. & Hafner, J. First-principles investigation of phase stability in  $\text{Li}_x\text{CoO}_2$ . *Phys. Rev. B* **58**, 2975–2987 (1998).
4. Van der Ven, A., Aydinol, M. K. & Ceder, G. First-principles evidence for stage ordering in  $\text{Li}_x\text{CoO}_2$ . *J. Electrochem. Soc.* **145**, 2149–2155 (1998).
5. Carlier, D., Van der Ven, A., Delmas, C. & Ceder, G. First-principles investigation of phase stability in the O-2-LiCoO<sub>2</sub> system. *Chem. Mater.* **15**, 2651–2660 (2003).
6. Chen, Z. H., Lu, Z. H. & Dahn, J. R. Staging phase transitions in  $\text{Li}_x\text{CoO}_2$ . *J. Electrochem. Soc.* **149**, A1604–A1609 (2002).
7. Gabrisch, H., Yazami, R. & Fultz, B. The character of dislocations in  $\text{LiCoO}_2$ . *Electrochem. Solid State Lett.* **5**, A111–A114 (2002).
8. Edwards, P. P., Rao, C. N. R. & Mott, N. F. *Metal–Insulator Transitions Revisited* (Taylor & Francis, London, UK; Bristol, Pennsylvania, USA, 1995).
9. Edwards, P. P. & Rao, C. N. R. *The Metallic and Nonmetallic States Of Matter* (Taylor & Francis, London; Philadelphia, 1985).
10. Graetz, J. *et al.* Electronic structure of chemically-delithiated  $\text{LiCoO}_2$  studied by electron energy-loss spectroscopy. *J. Phys. Chem. B* **106**, 1286–1289 (2002).
11. Reimers, J. N. & Dahn, J. R. Electrochemical and in situ X-ray-diffraction studies of lithium intercalation in  $\text{Li}_x\text{CoO}_2$ . *J. Electrochem. Soc.* **139**, 2091–2097 (1992).
12. Ohzuku, T. & Ueda, A. Solid-state redox reactions of  $\text{Li}_x\text{CoO}_2$  (R3m) for 4 volt secondary lithium cells. *J. Electrochem. Soc.* **141**, 2972–2977 (1994).
13. Shao-Horn, Y., Vlasseur, S., Weill, F. & Delmas, C. Probing lithium and vacancy ordering in O3 layered  $\text{Li}_x\text{CoO}_2$  ( $x \approx 0.5$ ). An electron diffraction study. *J. Electrochem. Soc.* **150**, A366–A373 (2003).
14. Amatucci, G. G., Tarascon, J. M. & Klein, L. C.  $\text{CoO}_2$ , the end member of the  $\text{Li}_x\text{CoO}_2$  solid solution. *J. Electrochem. Soc.* **143**, 1114–1123 (1996).

15. Menetrier, M., Saadouni, I., Levasseur, S. & Delmas, C. The insulator-metal transition upon lithium deintercalation from  $\text{LiCoO}_2$ : electronic properties and Li-7 NMR study. *J. Mater. Chem.* **9**, 1135–1140 (1999).
16. Molenda, J., Stoklosa, A. & Bak, T. Modification in the electronic-structure of cobalt bronze  $\text{Li}_x\text{CoO}_2$  and the resulting electrochemical properties. *Solid State Ionics* **36**, 53–58 (1989).
17. Imanishi, N., Fujiyoshi, M., Takeda, Y., Yamamoto, O. & Tabuchi, M. Preparation and Li-7-NMR study of chemically delithiated  $\text{Li}_{1-x}\text{CoO}_2$  ( $0 < x < 0.5$ ). *Solid State Ionics* **118**, 121–128 (1999).
18. Anderson, P. W. Absence of diffusion in certain random lattices. *Phys. Rev.* **109**, 1492 (1958).
19. Kittel, C. *Introduction to Solid State Physics* (Wiley, New York, 1996).
20. Kresse, G. & Furthmuller, J. Efficiency of ab-initio total energy calculations for metals and semiconductors using a plane-wave basis set. *Comp. Mater. Sci.* **6**, 15–50 (1996).
21. Kresse, G. & Furthmuller, J. Efficient iterative schemes for ab initio total-energy calculations using a plane-wave basis set. *Phys. Rev. B* **54**, 11169–11186 (1996).
22. Kresse, G. & Joubert, D. From ultrasoft pseudopotentials to the projector augmented-wave method. *Phys. Rev. B* **59**, 1758–1775 (1999).
23. Blochl, P. E. Projector augmented-wave method. *Phys. Rev. B* **50**, 17953–17979 (1994).
24. Aydinol, M. K., Kohan, A. F., Ceder, G., Cho, K. & Joannopoulos, J. Ab initio study of lithium intercalation in metal oxides and metal dichalcogenides. *Phys. Rev. B* **56**, 1354–1365 (1997).
25. Wolverton, C. & Zunger, A. First-principles prediction of vacancy order-disorder and intercalation battery voltages in  $\text{Li}_x\text{CoO}_2$ . *Phys. Rev. Lett.* **81**, 606–609 (1998).
26. Marianetti, C. A., Kotliar, G. & Ceder, G. Role of hybridization in  $\text{Na}_x\text{CoO}_2$  and the effect of hydration. *Phys. Rev. Lett.* **92**, 196405 (2004).
27. Hettler, M. H., Mukherjee, M., Jarrell, M. & Krishnamurthy, H. R. Dynamical cluster approximation: Nonlocal dynamics of correlated electron systems. *Phys. Rev. B* **61**, 12739–12756 (2000).
28. Biroli, G. & Kotliar, G. Cluster methods for strongly correlated electron systems. *Phys. Rev. B* **65** (2002).
29. Biermann, S., Aryasetiawan, F. & Georges, A. First-principles approach to the electronic structure of strongly correlated systems: Combining the GW approximation and dynamical mean-field theory. *Phys. Rev. Lett.* **90** (2003).
30. Sun, P. & Kotliar, G. Extended dynamical mean-field theory and GW method. *Phys. Rev. B* **66** (2002).
31. Dobrosavljevic, V., Pastor, A. A. & Nikolic, B. K. Typical medium theory of Anderson localization: A local order parameter approach to strong-disorder effects. *Europhys. Lett.* **62**, 76–82 (2003).
32. Mott, N. F. On the transition to metallic conduction in semiconductors. *Canad. J. Phys.* **34**, 1356 (1956).
33. Mott, N. F. *Metal-Insulator Transitions* (Taylor & Francis; Barnes & Noble Books, London, New York, 1974).

#### Acknowledgements

This research was supported with funding from the Department of Energy Basic Energy Science contract DE-F602-96ER45571, the National Science Foundation (NSF) Materials Research Science and Engineering Center program, and NSF contract DMR-0096462. We also gratefully acknowledge computing resources from the National Partnership for Advanced Computational Infrastructure. Correspondence and requests for materials should be addressed to G.C.

#### Competing financial interests

The authors declare that they have no competing financial interests.